Table 2 Overshoot and undershoot errors

t, sec	Tool left	Tool right
0–0.2	Undershoot	Overshoot
0.2–0.75	Overshoot	Undershoot
0.75–end	Undershoot	Overshoot

generated using dynamic optimization techniques which have been widely discussed in the literature.[3]

References

[1] Lewis, E. E. and Stern, H., *Design of Hydraulic Control Systems* (McGraw-Hill Book Company Inc., New York, 1962).

[2] Ellert, F. J., "Indices for control system design using optimization theory," Doctoral Thesis, Rensselaer Polytechnic Inst., Troy, N.Y. (January 1964).

[3] Merriam, C. W., III, *Optimization Theory and the Design of Feedback Control Systems* (McGraw-Hill Book Company Inc., New York, 1964).

NOVEMBER 1967 J. SPACECRAFT VOL. 4, NO. 11

Calculated Aeroelastic Bending of a Sounding Rocket Based on Flight Data

GEORGE E. REIS* AND WAYNE D. SUNDBERG†
Sandia Laboratory, Albuquerque, N. Mex.

During a series of Nike-Tomahawk sounding rocket flights, large extra-atmospheric coning angles were observed which were not predicted by preflight calculations. The most probable causes were concluded to be Magnus forces, aeroelastic bending, and/or lee-side boundary-layer separation. This paper is a report of an investigation of the aeroelastic behavior of one of these flights. An analysis was made which assumed that the missile consisted of two rigid bodies (payload and motor) hinged at their interface. Three-degree-of-freedom moment equations were written for each of the sections that were coupled by a bending moment at the hinge point. Sufficient data were available from flight, wind-tunnel, and laboratory tests to calculate the coning angles of each section. The maximum angular difference between the payload and the motor, immediately following second-stage burnout, was calculated to be $\frac{3}{4}°$. Flexural strengths obtained from bending tests accounted for the angular difference except for a 4-sec period near burnout. The additional bending is attributed to the opening of the payload separation joint caused by the rapid aerodynamic heating and sudden loss of acceleration at second-stage burnout.

Nomenclature

d = missile diameter, ft
I_{xn}, I_{yn} = moments of inertia of the payload about the x and y axes, respectively, in the payload coordinate system, slug-ft²
I_{xt}, I_{yt} = moments of inertia of the motor about the x and y axes, respectively, in the motor coordinate system, slug-ft²
K = payload-motor elastic flexural stiffness coefficient, rad/ft-lb
M_{bn} = hinge bending moment applied to the payload by the motor at the payload-motor joint, ft-lb
M_{xn}, M_{xt} = external moments applied about the x axes of the payload and motor, respectively, in their individual coordinate systems, ft-lb
$M_y(\theta_n), M_y(\theta_t)$ = aerodynamic moments applied about the y axes of the payload and motor, respectively, in their individual coordinate systems due to their respective angles of attack, ft-lb
$M_y(\dot{\theta}_n), M_y(\dot{\theta}_t)$ = aerodynamic moments applied about the y axes of the payload and motor, respectively, in their individual coordinate systems, due to the rate of change of their respective angles of attack, ft-lb
M_z = $M_{zn} + M_{zt}$, sum of the external moments applied about the z axes of the payload and motor, respectively, in their individual coordinate systems, ft-lb
q = dynamic pressure = $\rho V^2/2$, psf
V = missile velocity, fps
x, y, z = orthogonal body coordinates
X = distance between point P in Fig. 1 and the center of pressure of the payload section, ft
θ_n, θ_t = payload and motor coning angles, respectively, rad; these are assumed to equal their respective angles of attack
ρ = air density, slug/ft³
ρ_{62} = air density taken from Ref. 8, slug/ft³
ω_s = $\omega_s' - \omega_p \cos\theta_n$, rad/sec
ω_s' = inertial spin rate about the x axis, rad/sec
ω_p = missile coning rate, rad/sec

Presented at the AIAA Sounding Rocket Vehicle Technology Specialist Conference, Williamsburg, Va., February 27–March 1, 1967 (no paper number; published in bound volume of conference papers); submitted March 13, 1967; revision received July 14, 1967. The authors would like to thank W. B. Brooks for the suggestion to treat the missile as a two-body problem. This work was supported by the Atomic Energy Commission. [7.02, 7.08]

* Staff Member, Aero-Thermodynamics Department.

† Staff Member, Aero-Thermodynamics Department. Associate Member AIAA.

Introduction

OVER the past four years, a series of Nike-Tomahawk[2] sounding rockets with a variety of payloads has been launched by Sandia Laboratory. Preflight estimates of the behavior of the spinning missile in flight were made using a six-degree-of-freedom computer program. The observed

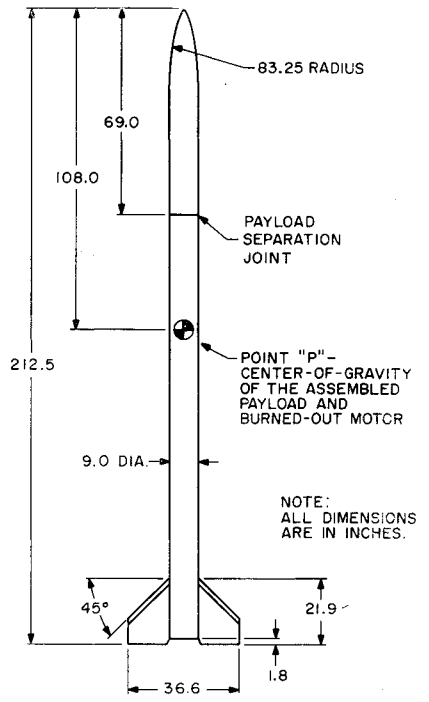

Fig. 1 Dimensions of flight 152-9 second stage.

flight behavior agreed quite well with the preflight predictions except for some rather large coning angles following second-stage burnout, which showed a tendency to vary radically from flight to flight. The computer calculations, using simple linear aerodynamics (rigid body, constant aerodynamic coefficients, etc.), predicted that for the burned-out motor and payload assembly shown in Fig. 1, the coning angle should not exceed 5° in the near-vacuum conditions above an altitude of 300,000 ft. For a group of 32 aerodynamically similar flights, this 5° maximum amplitude was exceeded in more than 40% of the flights, in one case exceeding 60° (Fig. 2).

During the early stages of the program there was considerable concern with the reasons for these unpredicted large coning angles. The three most likely causes were concluded to be Magnus forces, aeroelastic bending, and/or lee-side boundary-layer separation. Each of these possible causes was examined separately.[3–5] Roll-pitch coupling was discounted because of the marked difference between the roll and coning frequencies. Aeroelastic bending seemed likely because of the implications of Fig. 2. This plot was made by collecting the data according to each of the two types of payload-motor joints used in these flights, and computing a maximum coning-angle statistical frequency distribution curve for each type of joint. The data labeled "ball joints" in this plot had the payload-motor joint arrangement shown in Fig. 3 with the exception that the nosecone joint could be either a ball (separation) or radial screw joint. The data labeled "screw joints" had the same arrangement except that the payload separation ball joint in Fig. 3 had been replaced with a radial screw joint. Schematic drawings of the two types of joints are shown in Fig. 4. The work reported here is the result of the investigation to determine if aeroelastic bending could account for the observed behavior of one of the flights (152-9), using, wherever possible, experimental data from wind-tunnel tests, flight records, and laboratory tests.

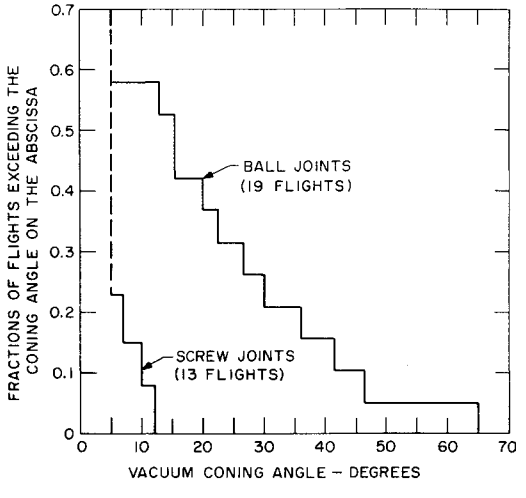

Fig. 2 Extra-atmospheric coning-angle frequency distributions.

A simplified bending analysis of the missile in flight was performed by assuming that the six-degree-of-freedom equations of motion could be decoupled and the missile treated as two rigid bodies hinged at the payload-motor separation joint. Using the available data, the motor angle of attack was calculated, using the rotational equations of motion, and compared with the observed payload angle of attack.

Static bending tests were also made on the payload and motor separately to determine if the difference in the coning angles of the payload and motor could be accounted for by the rigidity of the missile. From the coning-angle calculations enough information was acquired to evaluate all the terms in the equations of motion for moments applied to the payload and to the motor about the yaw and roll axes. From these a total yawing moment (which contains any Magnus and lee-side boundary-layer separation moments) was calculated and compared with the yawing moments calculated from Refs. 3–5.

Equations of Motion

Initially, an attempt was made to write the three-degree-of-freedom moment equations for the payload and for the motor in one coordinate system. The rather complicated set of equations that resulted indicated that it was more practical to divide the problem into two sections, one concerned with the behavior of the payload alone, and the other concerned with the motor alone. This resulted in choosing two sets of orthogonal axes shown in Fig. 5. For the payload, the x axis was chosen as the payload axis of symmetry, the z axis was set perpendicular to the x axis in the plane containing

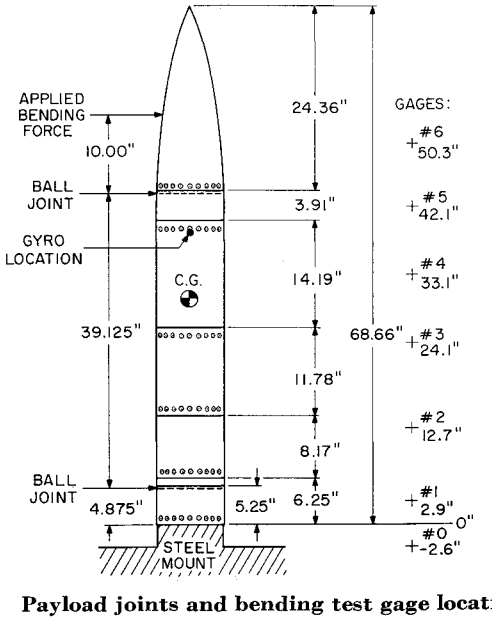

Fig. 3 Payload joints and bending test gage locations.

the x axis and the flight path, the y axis was set perpendicular to the x and z axes, and the origin was located at the intersection of the x axis and the flight path. For the motor, the x axis was chosen as the motor axis of symmetry, the z axis was set perpendicular to the x axis in the plane containing the x axis and the flight path, the y axis was set perpendicular to the x and z axes, and the origin was located at the intersection of the x axis and the flight path.

Because the method[6] of transforming the rotational equations of motion for a rigid body from the inertial set of axes to the axes systems just defined is straightforward, long, and tedious, the details of the transformation are omitted. The transformed equations of motion in the coordinate system attached to the payload were

$$I_{yn}\ddot{\theta}_n - (I_{yn} - I_{xn})\omega_p^2 \sin\theta_n \cos\theta_n + I_{xn}\omega_s\omega_p \sin\theta_n = M_y(\theta_n) + M_y(\dot{\theta}_n) + M_{bn} \quad (1)$$

$$(2I_{yn} - I_{xn})\omega_p\dot{\theta}_n \cos\theta_n + I_{yn}\dot{\omega}_p \sin\theta_n - I_{xn}\omega_s\dot{\theta}_n = M_{zn} \quad (2)$$

$$I_{xn}(\dot{\omega}_s + \dot{\omega}_p \cos\theta_n - \omega_p\dot{\theta}_n \sin\theta_n) = M_{xn} \quad (3)$$

The transformed equations of motion in the coordinate system attached to the motor were

$$I_{yt}\ddot{\theta}_t - (I_{yt} - I_{xt})\omega_p^2 \sin\theta_t \cos\theta_t + I_{xt}\omega_s\omega_p \sin\theta_t = M_y(\theta_t) + M_y(\dot{\theta}_t) - M_{bn} \quad (4)$$

$$(2I_{yt} - I_{xt})\omega_p\dot{\theta}_t \cos\theta_t + I_{yt}\dot{\omega}_p \sin\theta_t - I_{xt}\omega_s\dot{\theta}_t = M_{zt} \quad (5)$$

$$I_{xt}(\dot{\omega}_s + \dot{\omega}_p \cos\theta_t - \omega_p\dot{\theta}_t \sin\theta_t) = M_{xt} \quad (6)$$

Inherent in these equations are the assumptions that the payload and motor are spinning and coning at the same angular rate, the xz planes for the payload and motor coordinate systems are identical, the moment of inertia about the y axis is equal to that about the z axis for each of the missile sections, and all terms associated with products of inertia and rates of change of moments of inertia are negligible.

Flight Data

Missile flight 152-9 was fired at 11:00 AM (L.S.T.) on November 22, 1963, at Barking Sands, Kauai, Hawaii. The launch angle was 84°. First-stage burnout and separation occurred 3.55 sec after launch at an altitude of 4800 ft. The second stage was ignited at 16.2 sec at an altitude of 29,000 ft and burned out between 24.6 and 25.2 sec after launch at an altitude of 69,000 ft. The payload was separated at 55 sec after launch at an altitude of 277,000 ft and reached an apogee of 958,000 ft.

Values of the payload coning angle θ_n, the coning rate ω_p, and the rolling rate ω_s were obtained from the telemetry records of the output of the MARS[7] roll stabilized platform. A plot of ω_s and ω_p vs time is given in Fig. 6. Values of $\dot{\theta}_n$ and $\ddot{\theta}_n$ were calculated by applying a weighted smoothing and numerical differentiation to the θ_n data. These data were

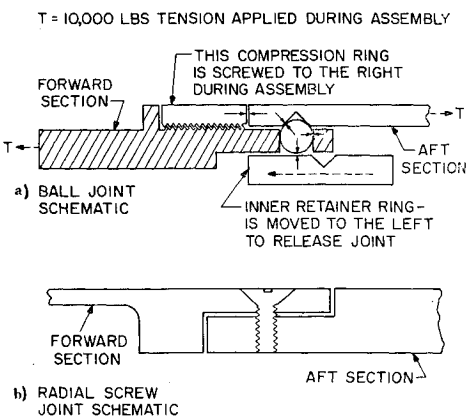

Fig. 4 Sectional diagrams of payload-motor joints.

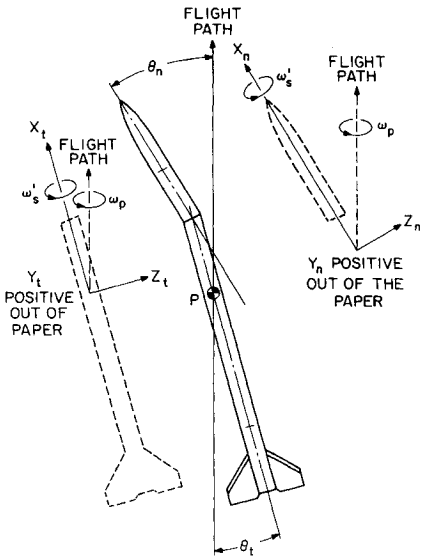

Fig. 5 Payload and motor coordinate systems.

assumed to represent the behavior of the payload at its center of gravity, since the payload center of gravity and the pitch and yaw sensing gyros were located in the same payload compartment. The accuracy of θ_n prior to smoothing has been estimated from an over-all systems check to be $\pm 0.1°$ (0.00175 rad). A qualitative examination of the smoothing procedures indicates that the error in θ_n should be reduced by smoothing. The velocity of the missile V and the altitude were obtained from calculations based on an FPS16 radar track of the missile. Over the period used in this analysis, the velocity varied between 6200 and 7600 fps.

Two weather balloon flights were flown on the day following flight 152-9. Because of the relatively stable nature of the atmosphere at the launch site, the data from these Rasonde flights were used to calculate the air density from sea level to an altitude of 117,000 ft on the day of the flight. The air density ratio (ρ/ρ_{62}), using the data from these balloon flights and the U.S. Standard Atmosphere[8] data, is plotted in Fig. 7 along with an estimate of the density profile above 117,000 ft altitude taken from published data for the time and place of the flight. With the exception of θ_n, $\dot{\theta}_n$, and $\ddot{\theta}_n$, all the flight data were assumed to represent the behavior of the motor as well as the payload.

Missile Characteristics

Laboratory measurements on the payload and a burned-out Tomahawk motor with attached fins, shown in Fig. 1, gave the data listed in Table 1. These values of weights, centers

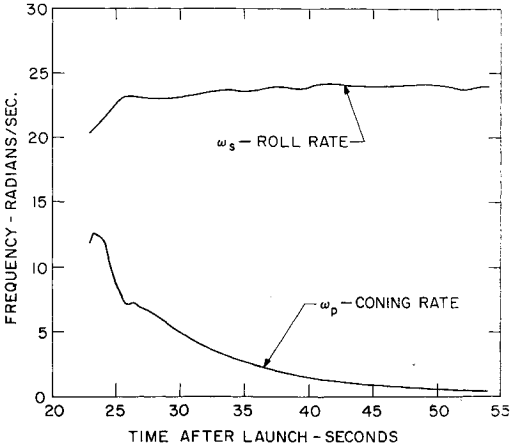

Fig. 6 Flight 152-9 roll and coning frequencies.

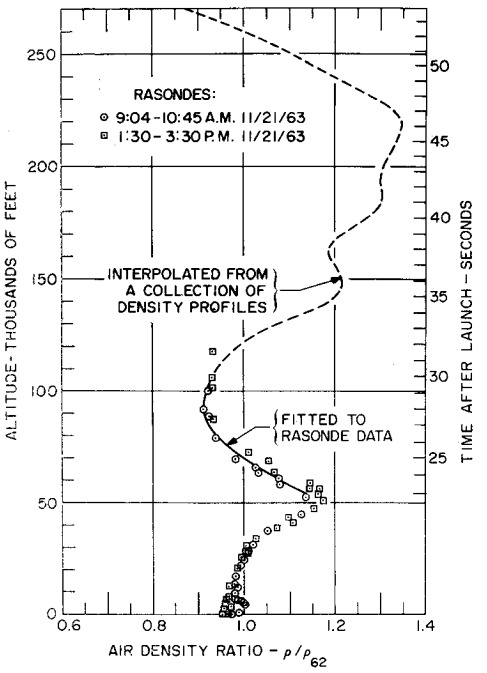

Fig. 7 Atmospheric density profiles.

of gravity, and moments of inertia were used in evaluating the various terms in the equations of motion. Although these values are reasonably accurate, the weight and moments of inertia were varying between 23.0 and 25.2 sec in the actual flight. This introduced an error into the calculations of a few percent over the first 2.2 sec of the analysis which was ignored, not being considered critical to the analysis since the primary concern was with the period after burnout. If the time-varying weights and moments of inertia had been included in the analysis, a much more complicated set of moment equations would have resulted.

Wind-Tunnel Tests

In order to determine the aerodynamic pitching moments as a function of the angle of attack for the payload and for the motor, two wind-tunnel tests were conducted.[9] The first was run on a $\frac{2}{9}$-scale model of the payload alone at a Mach number of 7.3 and Reynolds numbers, based on model length, between 1.5 and 2.0 $\times$ 10^6. Because the flight Mach numbers (6.3–8.0) did not vary appreciably from the wind-tunnel value between 23 and 54 sec, no correction was made to the wind-tunnel data for Mach number effects. Since Reynolds number effects were not determined for the range (135–0.01 $\times$ 10^6) covered by the flight over this same time period, no Reynolds numbers corrections were applied to the wind-tunnel data. The measured pitching moments were then transferred to the reference point P, the center of gravity of the burned-out, rigid payload-motor assembly in Fig. 1, and fitted by a least-squares fit to the data with a nonsymmetric cubic equation in $\sin\theta_n$. The resulting payload pitching-moment equation for the missile shown in Fig. 1 was

$$M_y(\theta_n) = q[8.8\sin\theta_n + 11.3\sin^2\theta_n + 14.4\sin^3\theta_n] \quad (7)$$

A payload aerodynamic pitch damping moment was calculated from the relation

$$M_y(\dot{\theta}_n) = -(X\dot{\theta}_n/V)(\partial/\partial\theta_n)[M_y(\theta_n)] \quad (8)$$

Individual values of $M_y(\dot{\theta}_n)$ were calculated and fitted with a quadratic equation in $\sin\theta_n$. The necessary values of X were taken from the wind-tunnel data. The resulting equation for the payload pitch damping moment was

$$M_y(\dot{\theta}_n) = -[q\dot{\theta}_n/V][63.4 + 134.1\sin\theta_n + 131.6\sin^2\theta_n] \quad (9)$$

A second wind-tunnel test[9] was run on a $\frac{1}{9}$-scale model of the complete payload-motor assembly at a Mach number of 7.3 and Reynolds numbers, based on model length, between 2.2 and 3.6 $\times$ 10^6. Although in the actual flight the missile was rolling, it was not possible to test a spinning model in the wind-tunnel tests. In order to make some estimate of the effects of rolling on the data from the nonrolling tests, the static moments were measured at each 5° of roll angle for every angle of attack. These varied by 10% for roll angles between 0° and 45°. These data were then transferred to the point P and fitted with a cubic equation in $\sin\theta_t$ giving the same statistical weight to each of the roll angles.† The equation for the payload pitch moment about point P obtained earlier was subtracted from this last equation to obtain an equation for the motor pitching moment about the point P. The resulting equation was

$$M_y(\theta_t) = -q[20.3\sin\theta_t + 9.00\sin^2\theta_t + 131.8\sin^3\theta_t] \quad (10)$$

A pitch damping moment for the motor was calculated in the same way as the pitch damping moment for the payload. The resulting equation for the motor pitch damping moment about the point P was

$$M_y(\dot{\theta}_t) = -[q\dot{\theta}_t/V][151.9 - 33.7\sin\theta_t + 1478.3\sin^2\theta_t] \quad (11)$$

No corrections were made to the total body wind-tunnel data for either Mach or Reynolds number effects.

Bending Tests

Static bending tests were made on the payload assembly shown in Fig. 3. Since attempts to analyze the payload as a simple cantilever beam were unsatisfactory, each section of the payload was assumed to be a rigid member with all deflection of the payload occurring at the joints between the sections. By fitting a mathematical expression for this model to the experimental deflection data, values of the stiffness coefficient for each of the two types of joints were calculated. Using these stiffness coefficients, a ratio between the base moment M_{bn} and the angular deflection of the center of gravity of the payload was calculated for a point load applied at the center of pressure. The motor was treated as a simple cantilever beam. Bending tests were made on both a pressurized and unpressurized motor case. The results were reduced, as with the payload, to a ratio between the base moment M_{bn} and the angular deflection of the motor case at its center of gravity.

Table 1 Measured weights, moments of inertia, and centers of gravity

	Payload	Burned-out motor with attached fins
Weight, lb	125	143
Center of gravity, ft aft of tip	3.1670	14.0993
Roll moment of inertia about vehicle axis, slug-ft^2	0.26 ($= I_{xn}$)	1.70 ($= I_{xt}$)
Pitch moment of inertia about center of gravity of the respective missile section, slug-ft^2	9.00	63.2
Pitch moment of inertia about center of gravity of payload and motor assembly,[a] slug-ft^2	141.20 ($= I_{yn}$)	178.76 ($= I_{yt}$)

[a] The center of gravity of the payload and burned-out motor assembly is 9.00 ft aft of the nose tip.

† This method of averaging over roll angle gives an $M_y(\theta_t)$ which is a reasonably accurate time average, provided the "effective" spin rate is large compared to the coning rate, i.e., $8\omega_s/\omega_p \gg 1$.

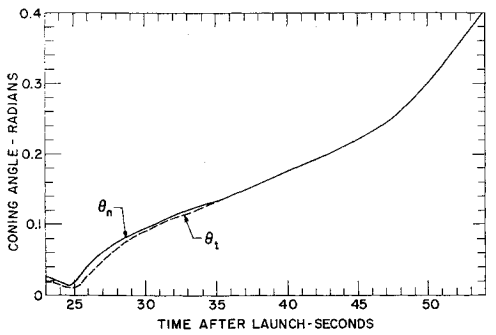

Fig. 8 Flight 152-9 payload (θ_n) and motor (θ_t) coning angles.

The angular deflections of the payload and motor were then combined to give the total angular deflection between the payload and motor centers of gravity. The final expression for the expected elastic angular deflection between the payload and motor for constant joint stiffness coefficients reduced to $-KM_{bn}$ rad, where $K = 2.91 \times 10^{-6}$ rad/ft-lb before burnout and 3.17×10^{-6} rad/ft-lb after burnout, and where M_{bn} is in ft-lb.

Numerical Calculations

Since the data necessary to evaluate the bending moment at the payload-motor joint were available for a period of time before and after second-stage burnout, the payload moment equation (1) about the pitch axis was combined with Eqs. (7) and (9) and then solved numerically for the hinge bending moment M_{bn} at every 0.2 sec from 2 sec before to 29 sec after burnout. The motor moment equation about the pitch axis, Eq. (4), combined with Eqs. (10) and (11) and the calculated values of M_{bn}, was then solved for the coning angle of the motor over this same time interval. These calculated motor coning angles θ_t are plotted along with the payload coning angles θ_n in Fig. 8. The expected elastic payload-motor flexure angle $-KM_{bn}$ was also calculated and is shown along with $(\theta_n - \theta_t)$ in Fig. 9.

As a result of the previous measurements and calculations, enough data were available to evaluate the left-hand side of Eqs. (2) and (5). These were evaluated to obtain the externally applied moments M_{zn} and M_{zt} about the z axes for the payload and the motor separately. The algebraic sum was then computed to obtain the total transverse moment M_z applied to the motor-payload assembly, which is shown in Fig. 10.

A subsidiary calculation was made by setting $\theta_t = \theta_n$, and then computing values of M_{bn} from the motor pitch equation (4). The results are plotted in Fig. 11 along with M_{bn} calculated from the payload pitch equation (1).

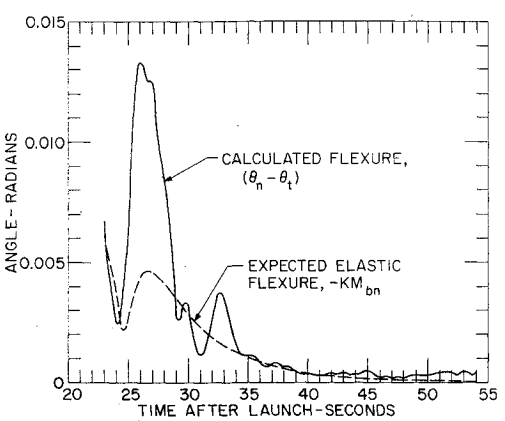

Fig. 9 Flight 152-9 calculated flexure and expected elastic flexure.

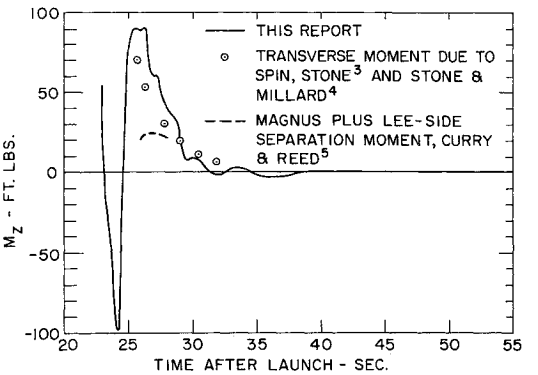

Fig. 10 Yawing moments calculated by various methods.

Discussion of Results

There appears to be little question that the missile was bent in flight because of the following. Since Eqs. (1) and (4) must be satisfied simultaneously, the same value of M_{bn} must appear in both equations at any given time in the flight. If θ_t is set equal to θ_n, the two values of M_{bn} computed from Eqs. (1) and (4) and plotted in Fig. 11 are appreciably different from 23 to about 30 sec after launch. From this it has been concluded that the missile was not rigid. The following discussion, therefore, is based on the values of θ_t computed for the bent missile.

Because the atmospheric density profile was determined by Rasonde balloon flights up to an altitude of 117,000 ft, corresponding to a time after launch of 32 sec, the calculated values of θ_t between 25 (second-stage burnout) and 32 sec are considered reliable. Between 32 and 54 sec, the calculated values of θ_t are less reliable since they are based on an estimated density profile.

To determine if the missile was behaving in flight as an elastic member, a comparison was made between $(\theta_n - \theta_t)$ calculated from the equations of motion, and the expected difference in the payload and motor coning angle $-KM_{bn}$, calculated from the missile stiffness. These are plotted together in Fig. 9. The plot shows reasonable agreement between the two curves except near the peak of $(\theta_n - \theta_t)$ shortly after second-stage burnout. The most logical explanation for the discrepancy between $(\theta_n - \theta_t)$ and $-KM_{bn}$ appears to be as follows.

Referring to Fig. 4, in the payload separation ball joint, the load applied during assembly causes a tension hoop stress in the outer member and a compression hoop stress in the inner member holding the two overlapping sections of the joint together. If it is assumed that during second-

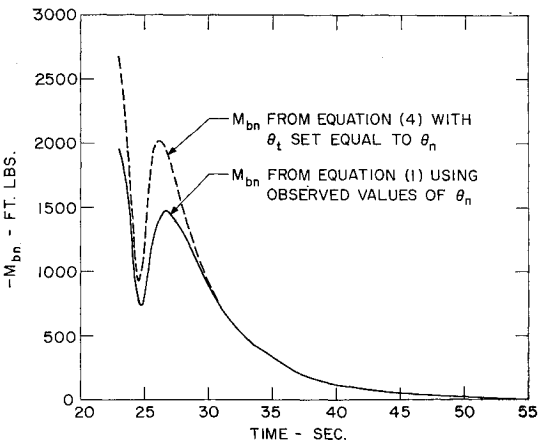

Fig. 11 Base moments calculated from payload and motor pitch equations.

Table 2 Comparison of flight and wind-tunnel test parameters

	Flight	Wind tunnel[5]
Reynolds number	$41.5\text{–}17.9 \times 10^6$	27.3×10^6
Mach number	7.76–7.11	5.0
Spin rate, rev/sec	3.7	0, 31.6, 47.5, 63.3
Fin cant, deg	0.28	0, 1.0, 1.5, 2.0
Pitching rate, deg/sec	0.8–1.2	0
Helix angle $= \omega_s d/2V$, deg	0.066	0, 0.37, 0.57, 0.76
Velocity, fps	7590–7482	2480
Coning rate, rev/sec	1.14–0.90	0

stage burning the outer section of the overlap is heated more rapidly than the inner section, the outer section will expand more rapidly than the inner one. This will relieve the hoop stresses and allow the joint to become partially or totally disengaged. During the period of second-stage burning, the acceleration due to thrust produces a moment which tends to reduce $(\theta_n - \theta_t)$. At second-stage burnout, this moment drops to zero and remains zero throughout the rest of the flight. As time goes on and the heating rate decreases, conduction through the joint will heat the inner section of the overlap, causing it to expand and close the gap between the two overlapping sections, thus reclosing the joint. Still later in the flight, both sections will tend to cool together (because of the decreasing air density), thereby keeping the joint closed. The sudden loss at burnout of the moment due to thrust combined with the loosened payload separation joint allows a sudden increase in $(\theta_n - \theta_t)$ immediately after second-stage burnout. Subsequent reclosing of the joint reduces $(\theta_n - \theta_t)$ to approximately the same value as $-KM_{bn}$. The rather close agreement between $(\theta_n - \theta_t)$ and $-MK_{bn}$ before burnout appears to justify the neglect of the variations in the moments of inertia in the moment equation calculations of θ_t.

The calculated values of the transverse moment M_z are useful in making a comparison between the results of the wind-tunnel tests of Curry and Reed[5] on a $\frac{2}{9}$-scale Tomahawk model and the work presented here. In order to make a direct comparison between their total lee-side boundary-layer separation plus the Magnus moments data with M_z, all of the conditions that existed in the wind-tunnel tests should be matched to the same conditions in the missile flight. There exists no part of the flight in which these conditions could be matched. However, near 27 sec after launch, two of the flight and wind-tunnel conditions, namely the Reynolds number ($\sim 27 \times 10^6$) and angle of attack ($\sim$0.05 rad), were the same. The Mach numbers (5 and $\sim$7.5) were reasonably close, but the remaining conditions were quite different. These conditions, whose relative importance is not known, are listed in Table 2. Because of the very small forces measured in the wind-tunnel tests, the listed values of the moment coefficient are subject to uncertainties which are not necessarily small. Also, from an examination of the wind-tunnel data, it was assumed that the transverse moment coefficient was not a strong function of the spin rate. Therefore, for the sake of comparison here, this coefficient was taken directly from Fig. 25 of Curry and Reed's[5] report.

Using these data, an estimate of the transverse moment due to the combined lee-side boundary-layer separation and Magnus moment was computed for the period between 26 and 28 sec after launch and is plotted as the short broken line in Fig. 10. As can be seen in the plot, this moment is appreciably less than the calculated values of M_z. The difference may be due to a variety of causes, such as the surface roughness, side slip, asymmetric flow, and/or other effects.

A more direct comparison can be made between the values of M_z computed from the bending analysis and the data of Stone[3] and Stone and Millard.[4] By combining the semi-empirical analysis of Stone[3] with the wind-tunnel results[4] and the appropriate flight data, transverse moments were computed that were attributed to Magnus effects. The results are plotted in Fig. 10 and are in reasonable agreement with the analysis developed in this paper. An extension of Stone's[3] analysis is given in a more recent paper.[10]

Roll-pitch coupling was eliminated from consideration because of the marked difference between ω_s and ω_p in Fig. 6. It is of interest to note that after this analysis was completed, a series of 10 Nike-Tomahawk flights has been made using very rigid separation joints. In these flights, the extra-atmospheric coning angles have all been less than 4°. A tabulation of the test data and the results of the calculations connected with flight 152-9 are given by Reis and Sundberg.[1]

Conclusions

From the results obtained in this investigation, the following is concluded. 1) Aeroelastic bending did occur on flight 152-9 and the maximum difference in the payload and motor coning angles was about $\frac{3}{4}$ deg in the pitch plane. 2) The flexure of the missile in the pitch plane can be accounted for by the elastic bending of the missile at all times between 23 and 54 sec after launch with the exception of a few seconds immediately following second-stage burnout where the bending appears to be inelastic. 3) The inelastic flexure of the missile appears to be due to the opening of the radially unconstrained payload separation ball joint when subjected to aerodynamic heating and loss of acceleration at second-stage burnout. 4) There existed a finite yawing moment whose cause or causes can not be determined by the foregoing bending analysis. 5) The yawing moment calculated from the bending analysis is in substantial agreement with the yawing moment calculated from wind-tunnel results and arguments that assign the yawing moment to the effects of spin. 6) Both the bending of the missile and the existence of a finite yawing moment are necessary conditions for the missile to have the observed coning history. 7) The analysis presented herein may be used with a fair degree of confidence to determine aeroelastic flexure of a missile having a relatively low joint stiffness.

References

[1] Reis, G. E. and Sundberg, W. D., "Calculations of the aeroelastic bending of a sounding rocket based on flight data," *AIAA Sounding Rocket Vehicle Technology Specialist Conference* (American Institute of Aeronautics and Astronautics, New York, 1967), pp. 402–422.

[2] Connell, G. M. and Stone, G. W., "Performance summary for the Sandia Nitehawk 9 rocket system," Sandia Lab. Rept. SC-RR-65-561 (July 1966).

[3] Stone, G. W., "The Magnus instability of a sounding rocket," AIAA Paper 66-62 (1966).

[4] Millard, W. A. and Stone, G. W., "The pitch damping characteristics of the Sandia Tomahawk rocket configuration," Sandia Lab. Rept. SC-RR-66-690 (July 1967).

[5] Curry, W. H. and Reed, J. F., "Measurements of Magnus effects on a sounding rocket model in a supersonic wind tunnel," AIAA Paper 66-754 (1966).

[6] *Vector Mechanics for Engineers*, combined edition, edited by H. R. Nara (John Wiley & Sons Inc., New York, 1962), Part I, pp. 296–299.

[7] Sinnot, N. F. and Rasmussen, R. O., "Performance and application of a miniature roll stabilized gyro platform," Sandia Lab. Rept. SC-R-65-1023 (October 1965).

[8] Dubin, M., Sissenwine, N., and Wexler, H., *U.S. Standard Atmosphere, 1962* (U.S. Government Printing Office, Washington, D.C., December 1962).

[9] Reece, E. W., "Results of wind tunnel tests to determine the effect of roll position on the longitudinal stability of the Tomahawk rocket configuration at Mach 7.3," Sandia Lab. Rept. SC-TM-66-495 (October 1966).

[10] Stone, G. W., "The angular motion of a rocket-propelled vehicle in free flight," Sandia Lab. Rept. SC-RR-66-42 (August 1966).